ACS Macro Letters

Letter

pubs.acs.org/macroletters

Noncovalent Functionalization of Graphene Nanosheets with Cluster-Cored Star Polymers and Their Reinforced Polymer Coating

Shan Wang, Haolong Li,* Dan Li, Tianyang Xu, Shilin Zhang, Xiaoyuan Dou, and Lixin Wu*

State Key Laboratory of Supramolecular Structure and Materials, College of Chemistry, Jilin University, Changchun 130012, China

Supporting Information

ABSTRACT: A noncovalent and phase-transfer-assisted method is developed for the fabrication of polymer-functionalized graphene, in which a series of cluster-cored star polymers (CSPs) containing a polyoxometalate core and polystyrene (PS) arms are used as modifiers. Through the electron transfer interaction between polyoxometalate and graphene, the CSPs can strongly adsorb on graphene nanosheets and transfer them from aqueous media to organic solvents like chloroform, forming individually dispersed graphene. Moreover, the CSP-functionalized graphene is well compatible with additional polymer matrices and can serve as a reinforcing nanofiller for polymer composites. A 0.2 wt% loading of them in PS coating achieves a 98.9% high enhancement in Young's modulus.

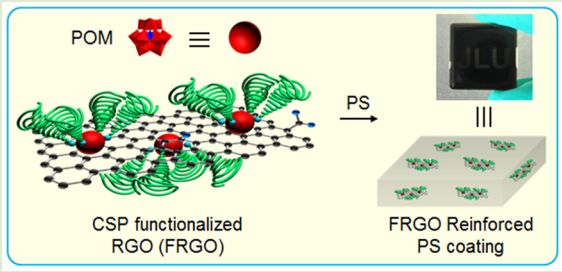

Graphene has attracted great interest owing to its unique two-dimensional structure and excellent properties.[1] Except for exploring its intrinsic properties, graphene is also used as a functional nanofiller for polymer nanocomposites.[2,3] A low loading of graphene in polymer matrices can dramatically improve the performance of polymer, ranging from mechanical reinforcement to enhanced electrical and thermal conductivity, etc.[4−8] However, the interaction between unmodified graphene and polymer is poor, therefore leading to a weak interface.[9,10] In this case, graphene tends to form irreversible agglomerates in polymer matrices, limiting the effective combination of their properties. Thus, improving the graphene−polymer interfacial compatibility is a key issue.

The surface chemical nature of graphene plays an important role in tailoring graphene−polymer compatibility. It is found that functionalizing the graphene surface with suitable polymer chains can effectively improve the interfacial compatibility between graphene nanosheets and polymer matrices.[2,3] On the basis of the reactive groups on graphene, polymer chains can be directly bonded through various organic reactions, such as the esterification with carboxyl or hydroxyl groups[11−14] and the radical addition with the carbon−carbon double bond,[15,16] leading to covalently grafted graphene. On the other hand, noncovalent modification is an alternative route to functionalize graphene, which primarily employs a hydrogen bond and $\pi-\pi$ interaction to adsorb polymers onto the graphene surface.[17,18] It allows the modification of graphene with the polymers bearing special structures or functions that need to be presynthesized and are difficult to bond covalently. For example, Tsitsilianis and co-workers used a PS_nP2VP_n star copolymer as an ionizable stabilizer to modify graphene through $\pi-\pi$ interaction, which conferred a responsibility to graphene.[18] Thereby, rationally utilizing noncovalent polymer modifiers is a facile and effective approach to prepare polymer-functionalized graphene.

Polyoxometalates (POMs) are the molecular clusters of a transition metal oxide, displaying a large structural variety, such as Lindqvist, Anderson, Keggin, and Dawson-type structures, as well as abundant properties in catalysis, electronics, magnetics, and medicine.[19] POMs are widely employed as versatile inorganic moieties to fabricate hybrid polymers.[20] Until now, a series of POM-containing polymers with linear,[21] star-like,[22−24] and network-like[25] structures have been synthesized and exhibit synergistic functionalities, such as enhanced luminescent[23,25] and catalytic properties.[21] Furthermore, recent studies reveal that POM clusters can strongly adsorb on the graphene surface to form hybrids,[26−31] driven by the electron-transfer (ET) interaction between POM and graphene.[29−31] On the basis of this property, POMs can serve as anchoring agents to modify other moieties onto graphene. Our group has successfully used surfactant-encapsulated POMs to functionalize graphene through the ET interaction, which can anchor the alkyl chains of surfactant on graphene and thus improve the organic dispersibility of graphene.[31] In light of this, herein we report a new method to prepare polymer-functionalized graphene by using POM cluster-cored star polymers (CSPs) as modifiers, as shown in Scheme 1. The CSPs can transfer reduced graphene oxide (RGO) from the water phase to organic solvents like chloroform, realizing the dispersion of individual RGO nanosheets. Moreover, the functionalized RGO is well compatible with additional polymer matrices and can be further used as nanofiller to prepare reinforced polymer coatings.

RGO nanosheets were prepared by a modified Hummers method and a subsequent reduction with hydrazine.[31,32] An

Received: April 30, 2015
Accepted: August 24, 2015
Published: August 25, 2015

DOI: 10.1021/acsmacrolett.5b00287
ACS Macro Lett. 2015, 4, 974−978

Scheme 1. Phase-Transfer-Assisted Fabrication of CSP-Functionalized RGO and Its PS Composite Coating

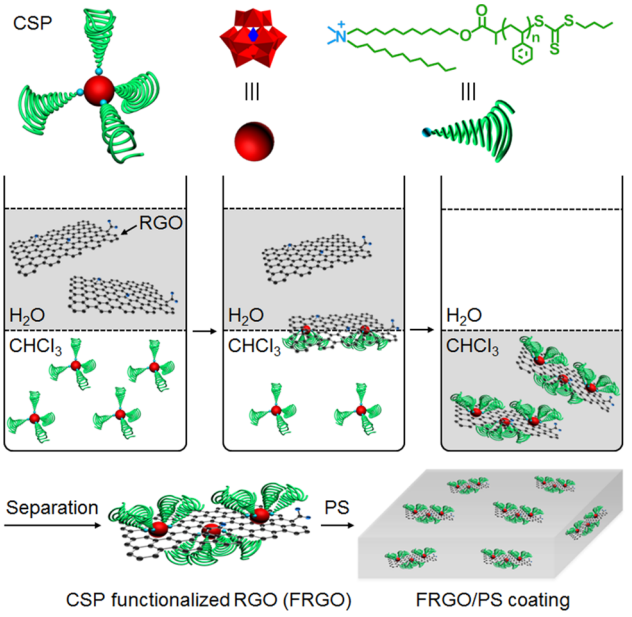

atomic force microscopy (AFM) image (Figure S1) shows that the size of GO is in the range from 200 to 400 nm, and the C 1s X-ray photoelectron spectroscopy (XPS) result (Figure S2) demonstrates that the content of oxygen-containing groups of RGO decreases from an initial 64.5% to 10.6% after reduction, reflecting an efficient reduction (Table S1). The thickness of the RGO nanosheet is about 1.08 nm (Figure S3), indicating that they are monolayers.[33] The CSPs were synthesized according to our previous method, and the whole synthetic procedure was shown in Scheme S1. A Keggin-type POM $H_4SiW_{12}O_{40}$ (SiW_{12}) was selected as the inorganic core, and then by RAFT polymerization, polystyrene (PS) arms were grafted from the chain transfer agent (CTA) premodified on SiW_{12} (see detailed characterizations in SI, Figures S4 and S5).[23] By adjusting the molar ratios of styrene to SiW_{12} from 100:1, 200:1, to 300:1, three CSPs (denoted as CSP-1, CSP-2, and CSP-3, respectively) with the same SiW_{12} core but different length of PS arms were obtained. Such a molecular design is aimed to investigate the influence of CSP hydrophobicity on their phase-transfer abilities. The successful polymerization was confirmed by ^{1}H NMR (Figure S6). The ^{1}H NMR spectra of three CSPs all show the characteristic proton signals of both the aromatic ring of the PS segment at 6.4−7.3 ppm and the two terminal $-CH_3$ groups of CTA at 0.8−1.0 ppm. Moreover, the integration ratio of PS to CTA becomes obviously larger when the polymerization is carried out at a higher molar ratio of styrene to SiW_{12}, indicative of an increasing length of grafted PS chains. Similar results were also supported by dynamic light scattering measurement (Figure S7), and the hydrodynamic diameters (D_h) are increased from CSP-1, CSP-2 to CSP-3. GPC measurement was further used to characterize the molecular weight of CSPs. To avoid that the star shape and the electrostatically bonded structure of CSPs affect the real elution time, we separated the PS arms from the SiW_{12} core by a reported column chromatography method.[23] SiW_{12} stayed in the silica gel column, and linear PS arms were obtained whose molecular weight can be easily measured by using linear PS as a reference due to their structural similarity. The M_n of the PS arms of CSP-1, CSP-2, and CSP-3 are 2.2, 3.5, and 5.6 kDa, respectively (Figure S8 and Table 1), which corresponds to the

Table 1. Summary of the GPC Data of Three CSPs

	molecular weight of PS segment on CSP arms			
	M_w/kDa	M_n/kDa	PDI	DP
CSP-1	2.4	2.2	1.09	15
CSP-2	3.7	3.5	1.06	28
CSP-3	6.1	5.6	1.09	48

degree of polymerization (DP) of 15, 28, and 48 after subtracting the CTA part. The PDI values are all below 1.10, reflecting a narrow distribution of PS arms. By using the DP values to fit the elemental analysis results of CSPs (Table S2), we inferred that the arm numbers of CSPs are all four, which means that the four CTA molecules on the periphery of SiW_{12} are all initiated during the RAFT polymerization process. FTIR spectra (Figure S9) of CSPs show the characteristic peaks of SiW_{12}, confirming the maintained framework of SiW_{12} in CSPs. Meanwhile, the vibrational bands of PS segments appear at 758 cm^{-1} (5 adj. H wag.) and 699 cm^{-1} (ring wag.), which become strong with the increasing length of PS chains.[23]

According to our previous work, CSPs possess a typical amphiphilic feature and can be stably spread onto the air−water interface.[23] This property enables CSPs as suprasurfactants to transfer RGO from aqueous solution to organic solvents like chloroform (Figure S10). The phase-transfer abilities of CSPs were systematically investigated by comparing CSPs with different molecular weights, as shown in Figure 1. The CTA-

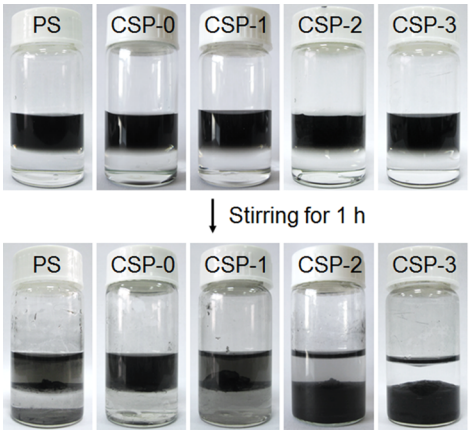

Figure 1. Photographs of phase-transfer experiments conducted using RGO (0.25 mg, 5 mL of H_2O) and CSPs or PS as phase-transfer agents (5 mL of chloroform). The weight ratios of CSPs or PS to RGO are all 20:1.

modified SiW_{12} can be regarded as the shortest CSP (denoted as CSP-0). It failed to transfer RGO due to the lack of hydrophobicity, consistent with our previous work where the POMs modified by short chain surfactants cannot carry out an effective transfer as well.[31] Interestingly, the CSPs exhibit a gradually changed phase-transfer ability depending on the length of their PS arms. In the case of CSP-1 whose arms have a DP value of 15, no RGO nanosheets were transferred to the chloroform phase. As for CSP-2 (DP = 28), the phase transfer occurred, but a few RGO nanosheets still remained in the water phase. For CSP-3 (DP = 48), it could transfer RGO from water to chloroform completely. The static contact angles of the

DOI: 10.1021/acsmacrolett.5b00287
ACS Macro Lett. 2015, 4, 974−978

CSPs increase with the increasing length of their arms (Figure S11), implying a gradually enhanced hydrophobicity of CSPs. These results demonstrate that only the CSP arms reaching a certain length can create enough hydrophobicity for the successful phase transfer of RGO. Additionally, to confirm the important role of the strong POM−graphene ET interaction in the phase transfer, neat PS was used as a comparison to transfer RGO. However, it failed even when the PS has a very high molecular weight (M_n = 170 kDa). This result demonstrates that only the $\pi-\pi$ interaction between PS and RGO cannot induce the occurrence of phase transfer. Thus, the POM−graphene ET interaction should be the predominant driving force for the phase transfer.

We further studied the influence of CSP amount on the phase transfer of RGO. CSP-3 was chosen as an example. As shown in Figure S12, when the weight ratio of CSP-3 to RGO is 1:1, phase transfer can occur, but a few remaining RGO nanosheets were still observed in the water phase, meaning a critical amount of CSP. At this condition, the transferred RGO should adsorb the lowest amount of CSP that satisfies the phase-transfer requirement. Further increasing the weight ratio to 2:1 and 3:1 can result in a complete transfer of RGO to chloroform, indicating an adequate amount of CSP. Therefore, it is possible to adjust the grafting density of CSP on RGO by controlling CSP amounts. On the basis of this, we prepared three CSP-functionalized RGO samples through varying the weight ratio of CSP-3 to RGO from 1:1, 2:1, to 3:1, denoted as FRGO-1, FRGO-2, and FRGO-3, respectively (see detailed procedures in SI). The ET interaction between SiW_{12} and RGO was confirmed by XPS spectra (Figure S13). The $W^{VI}4f_{5/2}$ and $W^{VI}4f_{7/2}$ peaks of FRGO-3 both shift to lower binding energies compared with those of CSP-3, reflecting that the electron density of the SiW_{12} core of CSP-3 has changed after being adsorbed on RGO.[29−31] Thermogravimetric analysis (TGA) was further used to evaluate the grafting content of CSP-3 on FRGO, as shown in Figure 2a, and Figure S14 shows that no

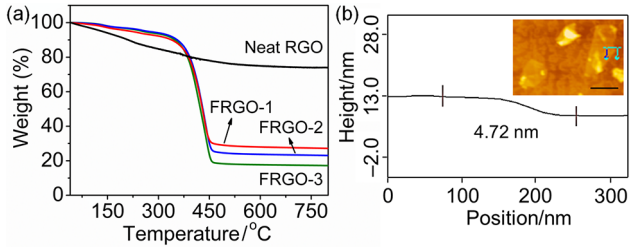

Figure 2. (a) TGA curves of RGO, FRGO-1, FRGO-2, and FRGO-3 (10 °C min^{-1} in N_2). (b) AFM height profile of FRGO-3 on the HOPG substrate (inset, scale bar: 500 nm).

free CSPs can be observed outside of the RGO nanosheets, indicating most CSPs were adsorbed on the RGO nanosheets. For neat RGO, its weight residual is 74.5% at 650 °C due to the removal of a few oxygen-containing groups. In comparison, the residual mass of FRGO-1, FRGO-2, and FRGO-3 is only 28.0%, 23.7%, and 17.7%, respectively, because the organic part of the CSP is decomposed under this condition. Assuming that all the residuals in FRGO are the thermal reduced RGO, WO_3, and SiO_2, the calculated contents of RGO are 26.1%, 19.2%, and 9.7% for FRGO-1, FRGO-2, and FRGO-3, respectively, which corresponds to the weight ratios of CSP to RGO of 2.8, 4.2, and 9.3 (Table S3), indicating a tunable grafting density of the CSP. Furthermore, the thickness of FRGO-3 obtained from the AFM height profile is about 4.72 nm (Figure 2b), much larger than that of neat RGO which is normally 1 nm measured by AFM (Figure S3), also confirming the successful grafting of CSP-3 on RGO nanosheets.

The dispersion state of three FRGO samples in chloroform was investigated by UV-vis-NIR spectra by changing their concentrations, as shown in Figure S15. All the results exhibit straight linear relationships between the absorbance at 800 nm and the concentration of RGO, well obeying Beer's law, further demonstrating the good dispersibility of FRGO.[31] Upon casting the chloroform dispersions on copper grids, many single-layered FRGO nanosheets are observed under transmission electron microscopy (TEM), confirming the individually dispersed state of FRGO (Figure 3a, 3c, and 3e). As is well-

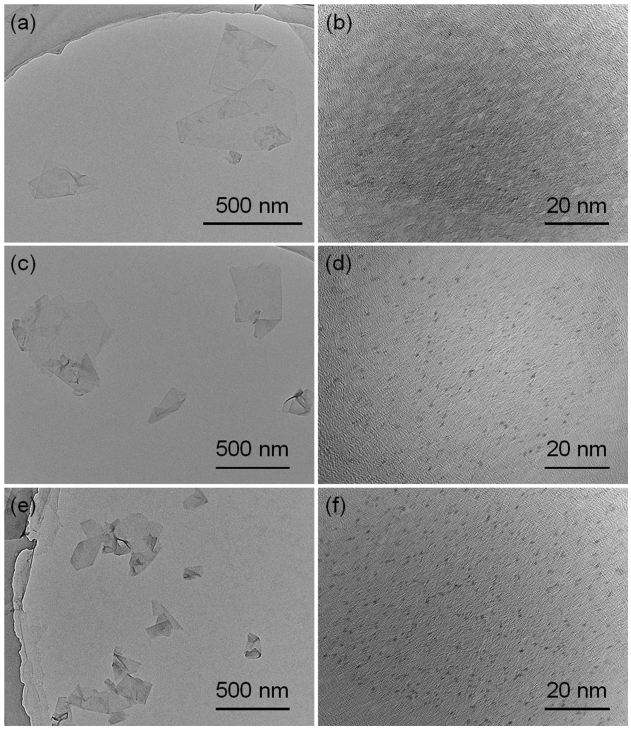

Figure 3. TEM images of (a, b) FRGO-1, (c, d) FRGO-2, and (e, f) FRGO-3.

known, common polymers show a very low contrast under the electron beam of TEM, and thus their grafting sites on graphene are usually difficult to be directly imaged by TEM. However, the CSPs in our work contain an inorganic SiW_{12} core which is easily observed by TEM due to its high content of heavy element tungsten and a visible size (about 1 nm). Taking this advantage, we can easily know the position of CSPs on FRGO nanosheets, as shown in Figure 3b, 3d, and 3f. Black dots about 1 nm in diameter are distributed on the nanosheets, which should be SiW_{12} clusters, as confirmed by energy-dispersive X-ray spectroscopy (EDX) with the presence of tungsten (Figure S16). This result realizes a direct visualization of the grafting sites on polymer-functionalized graphene. Moreover, TEM images show that the amount of SiW_{12} on FRGO nanosheets increased with the weight ratio of CSP-3 to RGO during the phase-transfer process, implying a tunable grafting density of CSP-3.

In view of its high Young's modulus, graphene is widely used as a nanofiller to enhance the mechanical properties of

DOI: 10.1021/acsmacrolett.5b00287
ACS Macro Lett. 2015, 4, 974−978

polymers.[2,3,5−7] However, most literatures regarding graphene−polymer nanocomposites were focused on the reinforcement of self-standing materials such as exfoliated casting films and hot pressed flakes, but only a few are related to polymer coatings.[34] Herein, we studied the mechanical property of FRGO-filled PS coatings. The good dispersibility of FRGO in chloroform allows us to incorporate them into PS matrix through a commonly used solvent-processing approach (see detailed procedures in SI). As shown in Figure S17 and S18, the neat PS coating is colorless and transparent, and the surface of the neat PS coating is very smooth. Upon adding FRGO and increasing their loading content from 0.05 to 0.2 wt%, the composite coatings become black gradually. However, even when the loading value reaches 0.2 wt%, the formed coating still remains transparent under strong visible light (inset in Figure 4b), indicating the good dispersibility of FRGO in the PS matrix.

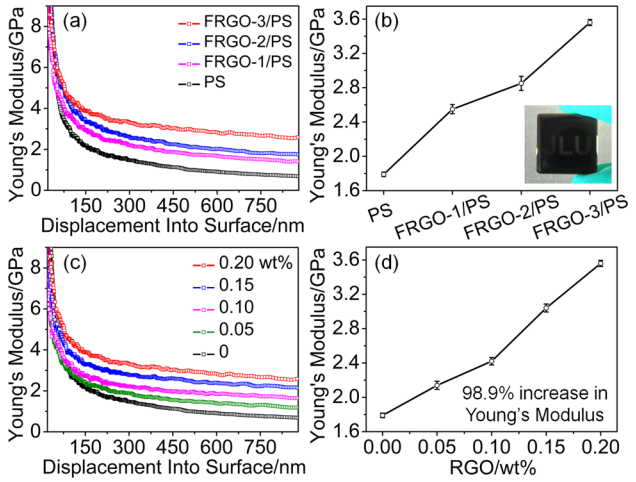

Figure 4. Young's modulus of the composite coatings as a function of indentation depth: (a, b) FRGO-1/PS, FRGO-2/PS, and FRGO-3/PS coatings with the same RGO content of 0.2 wt%; (c, d) the FRGO-3/PS coatings with increasing RGO contents from 0 to 0.2 wt%. Inset of b: a photograph of RGO-3/PS coating with 0.2 wt% RGO under strong visible light. The average values of Young's modulus in the approximate plateau region with an indentation depth from 150 to 300 nm in (a) and (c) are chosen for comparison.

In order to figure out the mechanical reinforcement of PS coatings brought by the loading of FRGO, their Young's modulus was measured using a nanoindentation technique, in which the neat PS coating shows a Young's modulus value of 1.79 GPa (Figure 4a). On one hand, we studied the influence of grafting density of CSP on the reinforcement (Figure 4a and 4b). Three coatings of FRGO-1/PS, FRGO-2/PS, and FRGO-3/PS were prepared with a constant RGO content of 0.2 wt% and showed an increasing Young's modulus from 2.55, 2.85 to 3.56 GPa. At this condition, the contents of RGO within the coatings are the same, and the only difference is the grafting density of CSP on RGO. Thereby, the increasing reinforcement should be attributed to the increasing grafting density of CSP. A higher grafting density is more favorable to achieve an adequate interaction of the RGO−PS interface. On the other hand, we investigated the influence of RGO loading on the reinforcement (Figure 4c and 4d). FRGO-3/PS is selected as the sample because its mechanical property is better than the other two. When the RGO contents in FRGO-3/PS coatings are varied from 0 to 0.2 wt%, a gradual enhancement in Young's modulus is observed. Without RGO, the CSP-3/PS coating shows a Young's modulus value of 1.60 GPa (Figure S19), and the neat CSP-3 almost has no effect on the glass transition, T_g, of the PS coating (Figure S20). These results indicate that the enhancement in Young's modulus is attributed to the intrinsically strong mechanical property of RGO. It should be noted that a high Young's modulus of 3.56 GPa is reached in the case of 0.2 wt% loading, which is 98.9% enhancement compared with neat PS coating.

In summary, we have presented a phase-transfer approach to prepare polymer-functionalized graphene, in which a series of POM-cored and PS-armed CSPs are used as modifiers, while the electron transfer interaction between POM and graphene is employed as a driving force. The functionalized graphene is not only dispersible in organic solvents as individual nanosheets but also well compatible with additional polymer matrices and can be used as a reinforcing nanofiller for PS composite coatings, realizing a 98.9% enhanced Young's modulus at a low loading of 0.2 wt%. These results pave a new way for functional graphene−polymer nanocomposites.

■ ASSOCIATED CONTENT

Supporting Information

The Supporting Information is available free of charge on the ACS Publications website at DOI: 10.1021/acsmacrolett.5b00287.

Detailed synthesis and characterizations (PDF)

■ AUTHOR INFORMATION

Corresponding Authors

*E-mail: hl_li@jlu.edu.cn.

*E-mail: wulx@jlu.edu.cn.

Notes

The authors declare no competing financial interest.

■ ACKNOWLEDGMENTS

This work was financially supported by the National Natural Science Foundation of China (51102112 and 21474039) and Jilin Provincial Science & Technology Department (201201013). We thank Ms. Y. Wang for nanoindentation measurements.

■ REFERENCES

(1) Geim, A. K.; Novoselov, K. S. *Nat. Mater.* **2007**, *6*, 183.
(2) Kim, H.; Abdala, A. A.; Macosko, C. W. *Macromolecules* **2010**, *43*, 6515.
(3) Potts, J. R.; Dreyer, D. R.; Bielawski, C. W.; Ruoff, R. S. *Polymer* **2011**, *52*, 5.
(4) Stankovich, S.; Dikin, D. A.; Dommett, G. H. B.; Kohlhaas, K. M.; Zimney, E. J.; Stach, E. A.; Piner, R. D.; Nguyen, S. T.; Ruoff, R. S. *Nature* **2006**, *442*, 282.
(5) Li, X.; McKenna, G. B. *ACS Macro Lett.* **2012**, *1*, 388.
(6) Liao, K. H.; Kobayashi, S.; Kim, H.; Abdala, A. A.; Macosko, C. W. *Macromolecules* **2014**, *47*, 7674.
(7) Beckert, F.; Held, A.; Meier, J.; Mülhaupt, R.; Friedrich, C. *Macromolecules* **2014**, *47*, 8784.
(8) Chen, Y.; Zhang, S.; Liu, X.; Pei, Q.; Qian, J.; Zhuang, Q.; Han, Z. *Macromolecules* **2015**, *48*, 365.
(9) Li, X.; Warzywoda, J.; McKenna, G. B. *Polymer* **2014**, *55*, 4976.
(10) Jiang, T.; Huang, R.; Zhu, Y. *Adv. Funct. Mater.* **2014**, *24*, 396.
(11) Salavagione, H. J.; Gómez, M. A.; Martínez, G. *Macromolecules* **2009**, *42*, 6331.
(12) Fang, M.; Wang, K.; Lu, H.; Yang, Y.; Nutt, S. *J. Mater. Chem.* **2009**, *19*, 7098.

DOI: 10.1021/acsmacrolett.5b00287
ACS Macro Lett. 2015, 4, 974−978

(13) Xu, Z.; Gao, C. *Macromolecules* **2010**, *43*, 6716.
(14) Yu, D.; Yang, Y.; Durstock, M.; Baek, J. B.; Dai, L. *ACS Nano* **2010**, *4*, 5633.
(15) Kan, L.; Xu, Z.; Gao, C. *Macromolecules* **2011**, *44*, 444.
(16) Liu, Z.; Xu, Z.; Hu, X.; Gao, C. *Macromolecules* **2013**, *46*, 6931.
(17) Liang, J.; Huang, Y.; Zhang, L.; Wang, Y.; Ma, Y.; Guo, T.; Chen, Y. *Adv. Funct. Mater.* **2009**, *19*, 2297.
(18) Popescu, M. T.; Tasis, D.; Tsitsilianis, C. *ACS Macro Lett.* **2014**, *3*, 981.
(19) Special issue on "Polyoxometalates". *Chem. Rev.* **1998**, *98*, 1−390.
(20) Qi, W.; Wu, L. *Polym. Int.* **2009**, *58*, 1217.
(21) Miao, W. K.; Yan, Y. K.; Wang, X. L.; Xiao, Y.; Ren, L. J.; Zheng, P.; Wang, C. H.; Ren, L. X.; Wang, W. *ACS Macro Lett.* **2014**, *3*, 211.
(22) Zhang, Q.; He, L.; Wang, H.; Zhang, C.; Liu, W.; Bu, W. *Chem. Commun.* **2012**, *48*, 7067.
(23) Li, D.; Li, H.; Wu, L. *Polym. Chem.* **2014**, *5*, 1930.
(24) Li, D.; Jia, X.; Cao, X.; Xu, T.; Li, H.; Qian, H.; Wu, L. *Macromolecules* **2015**, *48*, 4104.
(25) Li, H.; Qi, W.; Li, W.; Sun, H.; Bu, W.; Wu, L. *Adv. Mater.* **2005**, *17*, 2688.
(26) Li, H.; Pang, S.; Feng, X.; Müllen, K.; Bubeck, C. *Chem. Commun.* **2010**, *46*, 6243.
(27) Liu, R.; Li, S.; Yu, X.; Zhang, G.; Zhang, S.; Yao, J.; Keita, B.; Nadjo, L.; Zhi, L. *Small* **2012**, *8*, 1398.
(28) Tessonnier, J. P.; Goubert-Renaudin, S.; Alia, S.; Yan, Y.; Barteau, M. A. *Langmuir* **2013**, *29*, 393.
(29) Wen, S.; Guan, W.; Wang, J.; Lang, Z.; Yan, L.; Su, Z. *Dalton Trans.* **2012**, *41*, 4602.
(30) Wang, S.; Li, H.; Li, S.; Liu, F.; Wu, D.; Feng, X.; Wu, L. *Chem. - Eur. J.* **2013**, *19*, 10895.
(31) Wang, S.; Li, H.; Zhang, L.; Li, B.; Cao, X.; Zhang, G.; Zhang, S.; Wu, L. *Chem. Commun.* **2014**, *50*, 9700.
(32) Hummers, W. S.; Offeman, R. E. *J. Am. Chem. Soc.* **1958**, *80*, 1339.
(33) Li, D.; Müller, M. B.; Gilje, S.; Kaner, R. B.; Wallace, G. G. *Nat. Nanotechnol.* **2008**, *3*, 101.
(34) Yu, B.; Wang, X.; Xing, W.; Yang, H.; Song, L.; Hu, Y. *Ind. Eng. Chem. Res.* **2012**, *51*, 14629.

DOI: 10.1021/acsmacrolett.5b00287
ACS Macro Lett. 2015, 4, 974−978